



# OPEN Effect of dendritic structure on the filtration performance of fibrous media during dust loading by CFD-DEM

Yanju Li<sup>✉</sup>, Jixin Cui, Pengchang Chai & Yu Wang

Fibrous media filtration is effective to control particulate matter contamination in the air. To achieve filter performance precisely, the particle deposition with a 3-D fiber model was established based on the bag filter (F8) fibrous media and performed the effects of solid volume fraction (SVF), dust concentration and particle size on the filtration efficiency during the dust loading process by CFD-DEM. The results showed that the efficiency increased as the SVF of fibrous media increased. As particle size increased from 1  $\mu\text{m}$  to 120  $\mu\text{m}$ , the filtration efficiency improved from 51% to 97%. Filtration efficiency was proportional to the dust concentration and fluctuated at more than 90%. Furthermore, the dendritic structure affected filtration performance. The equivalent solid volume fraction (ESVF) was proposed, due to analyzing the collapse and reconstruction of dendritic structures during particle deposition. When the fluid velocity increased from 0.04 m/s to 0.21 m/s, the efficiency fell by around 20% because the dendritic structure of particles on the fiber was disrupted resulting in a reduction of the ESVF. These findings could provide aids to optimize the filtration performance and improve the indoor environment quality.

**Keywords** Fibrous media, Dendritic structure, Filter performance, ESVF, Dust loading

## Abbreviations

$\rho$	Density of the fluid ( $\text{kg}/\text{m}^3$ )
$g$	The acceleration of gravity ( $9.8 \text{ m}/\text{s}^2$ )
$u$	Fluid velocity ( $\text{m}/\text{s}$ )
$\epsilon$	The 3-D filter's porosity
$t$	Time (s)
$\tau$	Stress tensor (Pa)
$v$	Particles flow velocity ( $\text{m}/\text{s}$ )
$\omega$	Angular velocity ( $\text{rad}/\text{s}$ )
$I$	The moment of inertia of the particle ( $\text{m}^4$ )
$k$	The amount of collision of particles
$m$	The mass of the particle (kg)
$f_{fp}$	The force between the particle and fluid (N)
$f_{c,j}$	The tangential and normal contact force (N)
$f_{d,j}$	The tangential and normal damping force between the particles (N)
$T_j$	The torsional force produced by the collision of particles (N)
$c$	The solid volume fraction (SVF)
$\Delta c$	The equivalent solid volume fraction
$G_m$	Basic weight of fiber media ( $\text{kg}/\text{m}^2$ )
$X$	Thickness of the fiber media (mm)
$\rho_f$	The density of the fiber ( $\text{kg}/\text{m}^3$ )
$\Delta p$	The pressure drop between the two ends of the media (Pa)
$\mu$	The dynamic viscosity of the fluid ( $\text{kg}/(\text{m}\cdot\text{s})$ )
$d_f$	The fiber diameter ( $\mu\text{m}$ )
$f(c)$	A dimensionless function that reflects the impact of SVF

School of Energy and Safety Engineering, Tianjin Chengjian University, Tianjin 300384, China. ✉email: lindalyj@tcu.edu.cn

$Ku$	The kinetic factor of the Kuwabara flow field
$E\sum$	The total efficiency of a single fiber (%)
$V\sum$	The volume of the computational domain ( $m^3$ )
$V_f$	The volume of the fibrous media ( $m^3$ )
$V_p$	The volume of dendrites structure ( $m^3$ )
$M_{in}$	The mass of the imported particles (g)
$M_{out}$	The mass of the export particles (g)

Filtration is one of the most significant processes in mechanical gas-solid separation, as it separates scattered solid particles from a suspension. Air filters effectively remove outdoor pollutants and are primary for air conditioning systems to deal with fresh air<sup>1</sup>. Currently, the fibrous media is used for 70% of air filters<sup>2,3</sup>. Previous studies have found that the fiber structure and dust characteristics affect the properties of the fiber filter (pressure drop, efficiency, energy consumption, etc.).

Field studies have focused on the pressure drop of fiber filter materials. Meanwhile, a few researchers<sup>4–6</sup> have provided theoretical models for predicting pressure drop and an empirical formula for filtration efficiency to optimize the efficiency of a single fiber<sup>7</sup>. Saleh et al.<sup>8</sup> developed formulas for forecasting transient pressure decrease and evaluated the performance of pleated filters during dust loading. Subsequently, some studies have optimized the fiber material structures<sup>9,10</sup>. Li et al.<sup>11</sup> investigated the effect of fold shape on filtering performance and concluded that the fold ratio should be kept below 1.59. The filter materials were evaluated for filtration performance<sup>12</sup> and the particle's contribution to the filter's overall efficiency was determined using the single-fiber filtration efficiency model. Shu et al.<sup>13</sup> concluded that the transverse distribution of the amount of deposited particles in the pleated filter media was in two peaks structure. Zhang et al.<sup>14,15</sup> studied the performance of aircraft cabin air filters (V-type, cylindrical, and plate-type) and proposed an equivalent permeability coefficient method for determining the operating resistance of high-efficiency particulate air filters (HEPA). Zhang et al.<sup>16</sup> calculated the average pressure drop of the dust holding operation to determine the energy consumption of the HEPA media.

Furthermore, filters' performance and dust buildup distribution in dust-holding procedures have been investigated. Confocal microscopy has been used to observe the morphology and particle deposition caused by filter fiber material during the dusting process<sup>17</sup>. Cao et al.<sup>18</sup> simulated the dynamic change of pressure drop during dust loading are realized by CFD. Wang et al.<sup>19</sup> obtained the pressure drop of the filter material decreased as the dust loading rate increased for a specific filter area, experimentally. Besides, Yit et al.<sup>20</sup> found that the filtration efficiency increased with increasing velocity as the inertial impaction increased at higher velocity, experimentally. To summarize, experimental data on filtration performance and numerical models have been obtained in the dust loading process.

In numerical studies, filter media was simplified to single fiber or isolated fiber<sup>21,22</sup>. Based on the single fiber, the literature<sup>23,24</sup> analyzed the gas-solid flow of certain more regularly arranged fiber filters. To simplify the actual fiber filter to a regularly arranged structure, two-dimensional stochastic models have been utilized to characterize the filter material as a random column<sup>25</sup>. Kang et al.<sup>26</sup> has studied that the flow field of particles was simulated with the same fiber size, average solids and media thickness in a two-dimensional filter media model. However, the sampled two-dimensional model could not be effective in representing real fiber structures in the fiber filtration process.

Thus, the microscopic 3-D fiber model has been used to assess the impact of structural characteristics, operational parameters, and particle size on pressure drop and filtration efficiency<sup>16,27,28</sup>. Cao et al.<sup>29</sup> generated a 3D micro-scale model of fibrous media by the Voronoi algorithm. The effects of fiber structure<sup>12,30–32</sup>, particle diameter<sup>33</sup>, and airflow aerodynamic parameters on filter pressure drop<sup>19</sup> and efficiency<sup>33</sup> were explored with a 3-D fiber model created by CFD in field studies. Schilling et al.<sup>34</sup> compared the motion and redistribution of dendrite structures generated by sedimentary particles on filter fibers by using different multiphase methods, and obtained that the separation of dispersed particles in a fluid on single fiber of a fibrous media was determined by CFD-DEM. Previous studies<sup>35–37</sup> have reported that increasing fluid velocity and particle concentration could increase the capturing efficiency of a 3-D fiber model by the computational fluid dynamics-discrete element method (CFD-DEM). Vivacqua et al.<sup>38</sup> developed a rheological model that explains the relationship between the dimensionless shear stress and the inertial number for particle shapes. Dong et al.<sup>39</sup> established a particle interaction model to predict the dynamic deposition behavior by CFD-DEM. Cheng et al.<sup>40</sup> found that the CFD-DEM method could be applied to investigate the deposition process of pleated air filter media. Thus, CFD-DEM is a potent tool for analyzing gas-solid flow problems to improve solution accuracy in the capture efficiency by fibrous media.

The impact of fiber structure and dust source on the performance of the filter media dust-holding process has been studied, and some experimental data has been gained in previous studies. However, most of these investigations focused on the fiber structure of high-efficiency particulate air (HEPA) filters, and it is not enough to examine the deposition of medium-effect bag filters. Field studies on the deposition pattern of particles on the fiber surface and the process of "filter cake" formation have concentrated on the influence of dust loading on pressure drop and filtering efficiency. Besides, the effect of dust loading on fiber structure should be paid more attention in the deposition process. Due to the randomly distributed fibers and the unstable two-phase flow of gas and solids in the filtering process, this study aims to analyze the effect of changes in dendritic structure on SVF and filtration performance during dust loading by means of a stochastic 3D fiber model.

## Method

### Mathematical model

Aerosolized pollutant control by fibrous media is a dynamic process, in which the deposited particles continuously alter the pressure drop and efficiency. The Navier-Stokes equations have been used to solve the flow field and inter-particle interaction, and the Lagrangian equations have been used to solve particle motion.

#### Fluids

Fluid phase equations follow the mass conservation law and momentum conservation law of the local average variable. When simulating the dust loading in the filter, the air was treated as a continuous phase, expressed as the N-S Eqs. (1)–(2)<sup>41</sup>. For Reynolds number was less than 1, the airflow that passed through the fibrous media was considered as laminar.

$$\frac{\partial \varepsilon}{\partial t} + \nabla \cdot (\varepsilon u) = 0 \quad (1)$$

$$\rho \frac{\partial \varepsilon u}{\partial t} + \rho \nabla (\varepsilon u u) - \nabla \cdot (\varepsilon \tau) = -\varepsilon \nabla p + \rho \varepsilon g - f_{fp} \quad (2)$$

#### Particles

During particle deposition, the particles could interact with air and collide with fibers or adjacent particles, resulting in an exchange of momentum and energy. In this study, the JKR model<sup>42</sup> was adopted to solve the contact forces of particle-solid which is a non-linear soft-sphere model. The expressions were shown as follows<sup>43</sup>:

$$m \frac{dv}{dt} = \sum_{j=1}^k (f_{c,j} + f_{d,j}) + f_{fp} + mg \quad (3)$$

$$I \frac{dw}{dt} = \sum_{j=1}^k (T_j) \quad (4)$$

### Simulation method

In this study, the process of fine particles deposition and agglomeration was simulated by the CFD-DEM coupled model. The CFD method was calculated using Fluent software while the DEM method was calculated using EDEM software. In order to obtain a complete description of the interaction between fluid and particle, the two-way coupling which took the interactions of the particle-fluid and particle-particle into account was employed. A single particle could be tracked, yielding a wealth of information in a particle-fluid system based on the CFD-DEM model, which is critical for explaining the mechanics of particle-fluid flows. In the coupling process, the explicit time integration method was used to solve the translational and rotational motion of the particle in DEM, and the SIMPLE algorithm was adopted to solve the fluid control equations in CFD. The CFD-DEM models have been used to determine the state of motion of gases and particles in both the gas and solid phases<sup>36</sup>. The advantage of coupling computation is that it takes into account the particles' shape, characteristics, and size distribution, allowing the particles' movement and interaction with the fluid to be precisely defined. In this paper, several simplifications were applied to capture of particles as follows:

- (1) All particles are simplified to spherical;
- (2) No energy loss following the capture of particles;
- (3) Upon particle collision fibrous media is uniformly treated as was trapped, without satellite particle production, and only momentum is exchanged between the two particles without deformation.

### Structural model of fibrous media

#### The geometric models of fibrous media

To construct a more realistic fibrous media structure, the microscopic cross-sectional images of the interior filter media were obtained by scanning electron microscopy (SEM) imaging. Then, a text document containing the parameters, such as the diameter, bending, and position of the actual fiber extracted from the images, was written and identified to generate the 3-D fiber model automatically in CFD. In this paper, the 3-D model of fibrous medium constructed was an ordered model without considering fiber interlacing. Finally, 3-D models with random multilayer were established whose SVF were 1.84%, 2.9%, 4.09% and 5.28%, respectively. SVF is the fiber packing density, which was calculated as Eq. (5)<sup>51,52</sup>. The rendering of the 3-D model of fibrous media was shown in Fig. 1.

$$c = \frac{G_m}{\rho_f X} \quad (5)$$

#### Mesh independence validation

The mesh dependencies of the calculation model needed to be verified before the numerical calculation of the flow field was performed, which compared pressure drops at different fiber mesh densities to find an optimal solution<sup>46</sup>. Because the fibers were smaller than the computing domain, the increase in mesh number was necessary to improve the mesh quality<sup>47</sup>.

The results that pressure drop varied as the number of meshes<sup>46</sup> were shown in Fig. 2 (Fiber diameter ( $d_f$ ) = 7.66  $\mu\text{m}$  ~ 20  $\mu\text{m}$ . SVF = 0.0184). The pressure drop was stable when the number of meshes was about

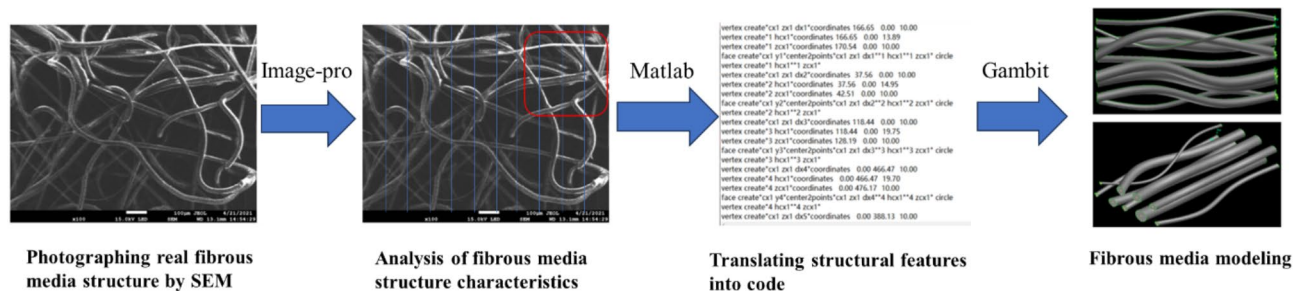


**Fig. 1.** The modeling process for 3-D fibrous media (Using the software is indicated above the arrow).

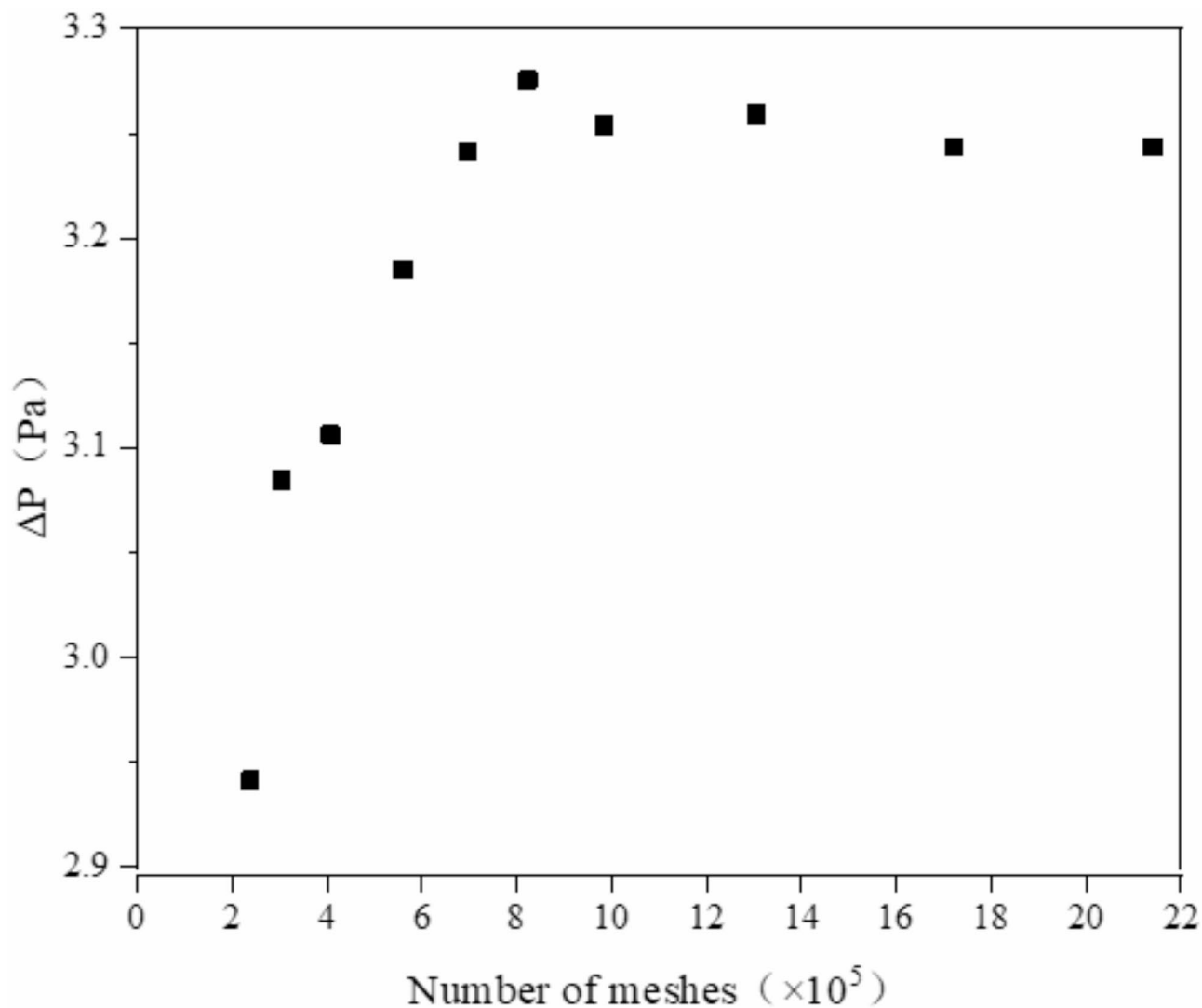


**Fig. 2.** Mesh independence test.

1 million in this case's calculation. In this study, mesh independence was demonstrated to result in mesh numbers ranging from approximately 1 million to 3 million in working conditions.

#### Model validation

To verify the usability and accuracy of the CFD model, the condition was selected (SVF = 5.28%, 1 layer of media) as an example. Figure 3 showed the comparison of the simulation values of pressure drop with the Kuwabara model values<sup>4</sup> and the Davies experimental correlation formula<sup>48</sup>. The numerical simulation value was well

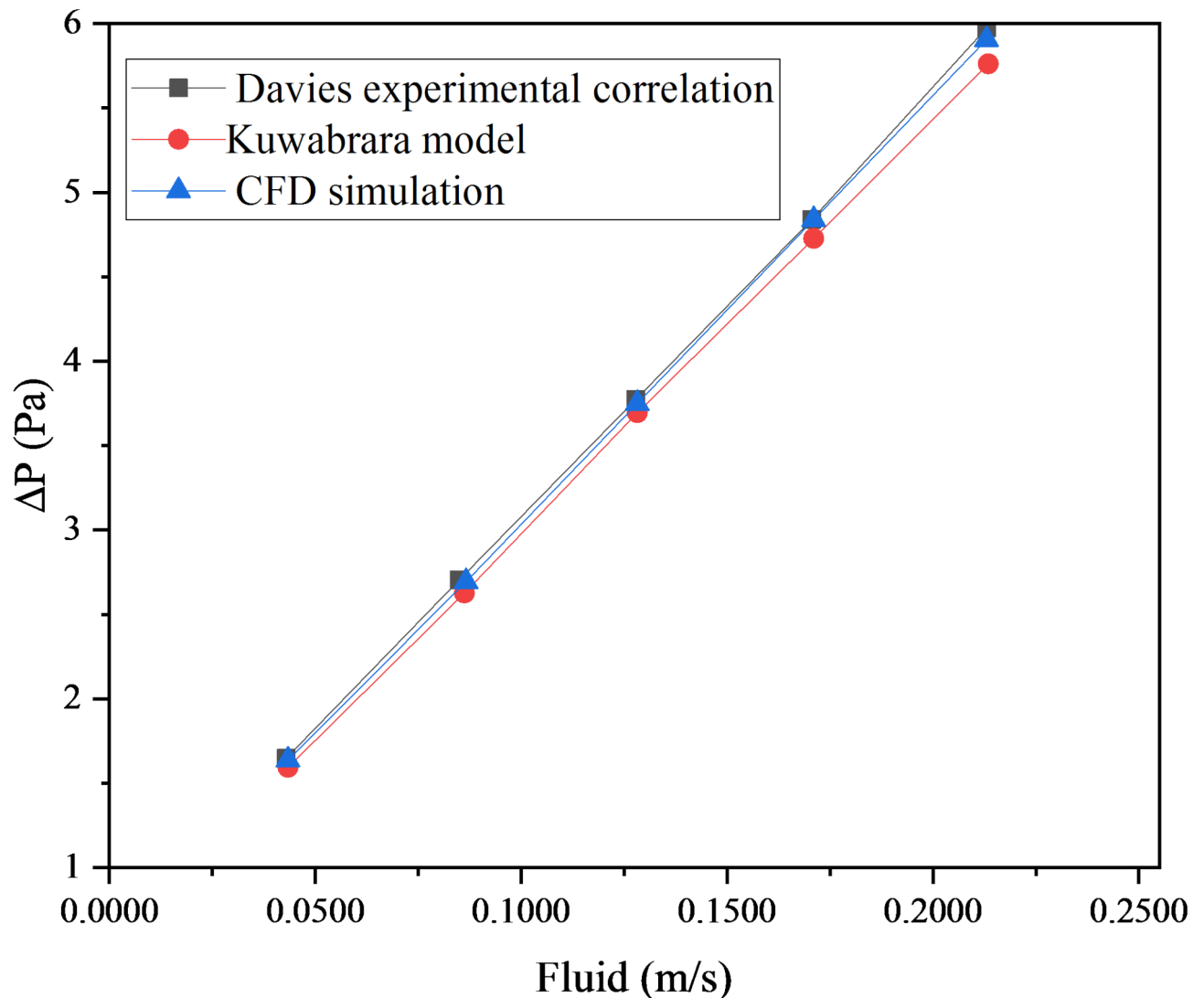


**Fig. 3.** Pressure drop comparison between CFD simulation and empirical models.

agreed with the empirical correlation value (Fig. 3), indicating that the calculation model was reasonable and the results were credible.

#### Computational domain and boundary conditions

Figure 4 showed the computational domain and boundary conditions of the numerical simulation model. The velocity-inlet and pressure-outlet were applied for the inlet and outlet of the airflow, respectively. The rest of the calculation region was subjected to periodic boundary conditions. The particle factory created and released particles at a distance of 0.05 mm from the surface of the 3-D filter media, which traveled with the fluid and were trapped by the fibrous media. Encapsulated particles exited the calculation area via the pressure outlet. The gas-solid two-phase flow was considered to be uniform and introduced into the computational area from the velocity input (left) to the pressure exit (right). In addition, non-slip boundary conditions were adopted with fiber surfaces. Tables 1 and 2 summarized the parameters used in the simulation.

#### Theoretical calculation

Regarding the resistance of the filter media of fiber filters, the airflow will be hindered when it passes through the filter media. At low flow rates and small Reynolds numbers, the pressure drop between the two ends of the porous media obeyed Darcy's law:

$$\Delta p = f(c) \frac{u \mu X}{d_f^2} \quad (6)$$

The most widely applied empirical formula derived by Davies<sup>19,56</sup>:

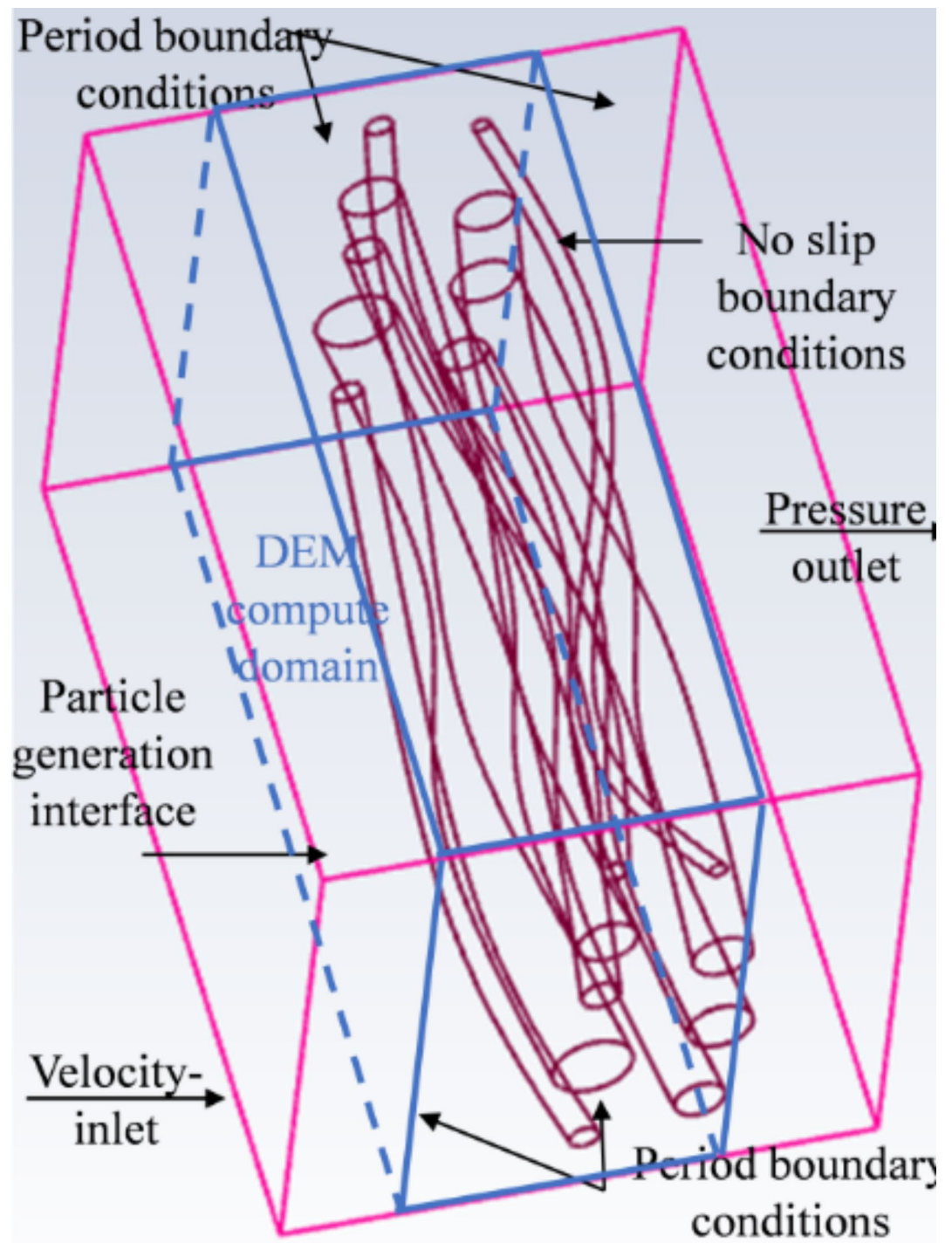


**Fig. 4.** Computational domain and boundary conditions.

Material	Particle	Fiber
Density(kg/m <sup>3</sup> )	900	800
Diameter(μm)	1–80	5–27
Poisson's ratio	0.21	0.4
Modulus of shear (MPa)	1	500

**Table 1.** The parameters of the material used in the simulation.

Interaction	Particle-particle	Particle-fiber
Coefficient of restitution	0.15	0.1
Coefficient of static friction	1	1
Coefficient of rolling friction	0.01	0.01

**Table 2.** The parameters of interaction used in the simulations.

	SVF(%)	Layer	fluid velocity (m/s)
Operation 1	1.84	1	0.04 0.09 0.13 0.17 0.21
Operation 2		2	
Operation 3		3	
Operation 4	2.90	1	
Operation 5		2	
Operation 6		3	
Operation 7	4.09	1	
Operation 8		2	
Operation 9		3	
Operation 10	5.28	1	
Operation 11		2	
Operation 12		3	

**Table 3.** The operating circumstances of the fiber media model.

$$f(c) = 64c^{3/2} (1 + 56c^3) \quad (7)$$

Kuwabara<sup>4</sup> analyzed and obtained the typical flow field applications by Darcy formula, which has the kinetic factors and dimensionless resistance as follows<sup>31,35</sup>:

$$f(c) = \frac{4c}{Ku} = \frac{4c}{-\frac{1}{2} \ln c + c - \frac{3}{4} - \frac{c^2}{4}} \quad (8)$$

The theoretical formula for filter media resistance under the Kuwabara flow field is:

$$\Delta p = \frac{4c}{-\frac{1}{2} \ln c + c - \frac{3}{4} - \frac{c^2}{4}} \frac{u\mu X}{d_f^2} \quad (9)$$

The filtration efficiency ( $E$ ) was expressed in Eq. (10)<sup>50</sup>.

$$E = 1 - \exp \left( \frac{-4\Delta c X E_\Sigma}{\pi d_f (1 - \Delta c)} \right) \quad (10)$$

The  $\Delta c$ , defined as Eq. (11), is the ESVF of fibrous media:

$$\Delta c = \frac{V_f + V_p}{V} \quad (11)$$

The  $V_p$ , defined as Eq. (12), is the volume of dendrites structure on the fibers during the filtration process. According to Eq. (12),  $V_p$  can be calculated for the mass  $M_{in}$  of the imported particles,  $M_{out}$  of the export particles and the density  $\rho$  of the A2 dust during dust loading.

$$V_p = \frac{M_{in} - M_{out}}{\rho} \quad (12)$$

## Results and discussion

In this section, the effects of fluid velocity (0.04 m/s, 0.09 m/s, 0.13 m/s, 0.17 m/s, and 0.21 m/s), a number of fibrous media layers, SVF (0.0184, 0.0290, 0.0409, and 0.0528) and dust accumulation were investigated on filtration performance, as well as dust deposition on fibrous media (Table 3). The fluid velocity range in the simulation as well as the SVF range are based on the EN779:2012<sup>51</sup>.

### The influence of SVF on pressure drop

Pressure drop is an important indicator to evaluate the performance of fibrous media. The simulated values of pressure drop at the fluid velocity were obtained for 12 operating circumstances and compared to determine the effect of SVF on the pressure drop of the fibrous media.

The pressure drop grew as SVF increased at the same fluid velocity. As the fluid velocity increased, the difference in pressure drop between the low SVF (0.0184) and high SVF (0.0528) was increased gradually. The pressure drop increased from 1.26 Pa (0.04 m/s) to 1.34 Pa (0.04 m/s) at the SVF of 0.0184 from 0.0528, while that increased from 4.48 Pa (0.17 m/s) to 5.74 Pa (0.17 m/s) at the same range of SVF. Under the fluid velocity of 0.21 m/s, the pressure drop increased from 5.52 Pa (0.0184) to 6.72 Pa (0.0528) in Fig. 5. The pressure drop grew also as fluid velocity increased at the same SVF. The pressure drop increased from 1.26 Pa (0.04 m/s) to 5.52 Pa (0.21 m/s) at the SVF of 0.0184, while that rose from 1.34 Pa (0.04 m/s) to 6.72 Pa (0.21 m/s) at the SVF of 0.0528 in Fig. 5.

According to Darcy's law, when a fluid flows through a porous media, the larger the input velocity, the greater the pressure gradient<sup>52</sup>, the pressure drop had a positive relationship with fluid velocity, and the change in pressure drop with fluid velocity was linear. The correlation formula indicated a positive correlation between pressure drop and SVF, which was consistent with the pattern in Fig. 5. Additionally, under higher velocity conditions, because dendrite structures were more likely to collapse, the pores were more easily clogged by particles, resulting in an increased pressure drop (Fig. 5). Yue et al.<sup>52</sup> showed that increasing the media SVF resulted in smaller pore sizes and a denser fiber arrangement in the fiber filter. The phenomenon results in increased obstruction of fluid flow, which leads to increased pressure drop.

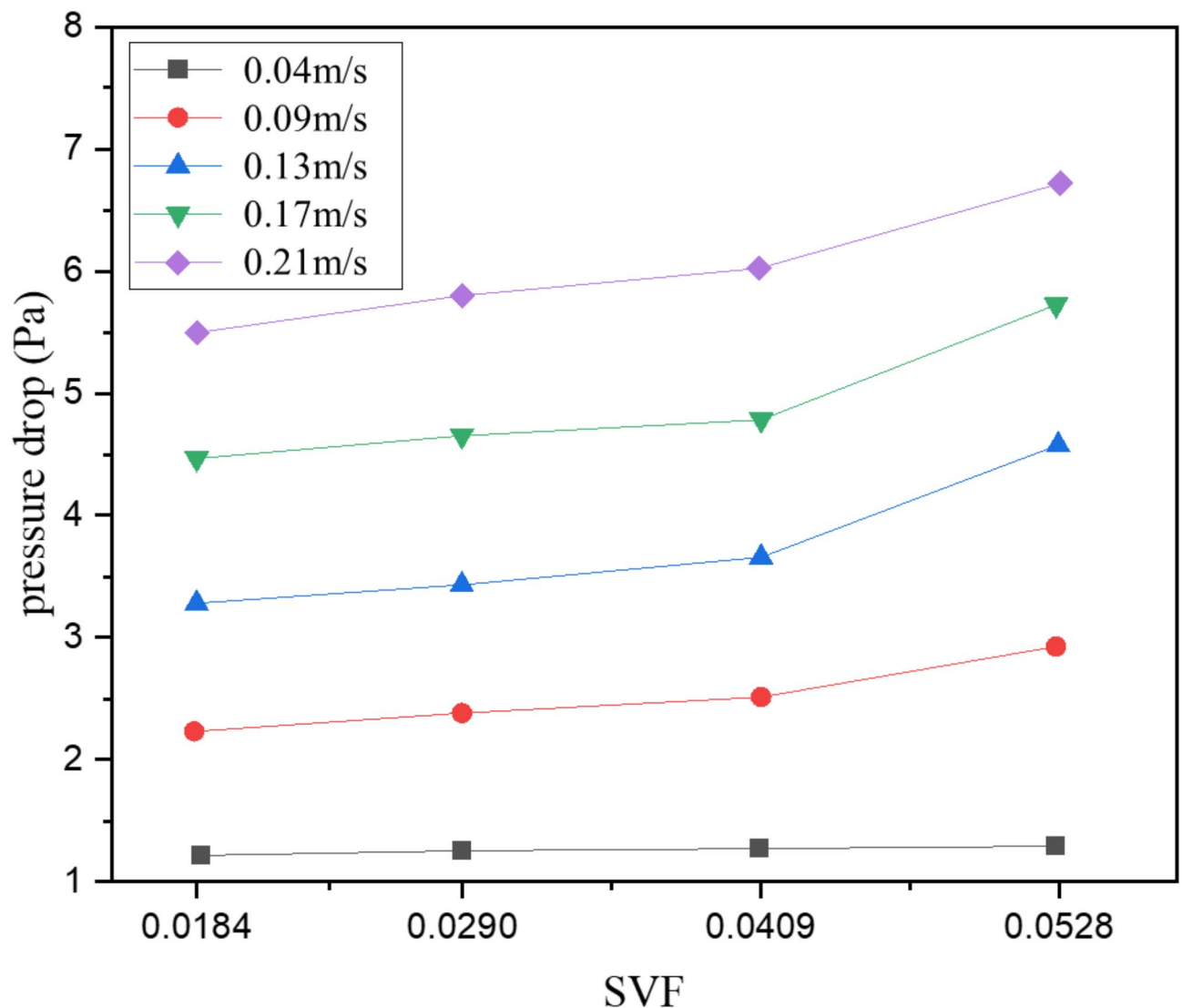
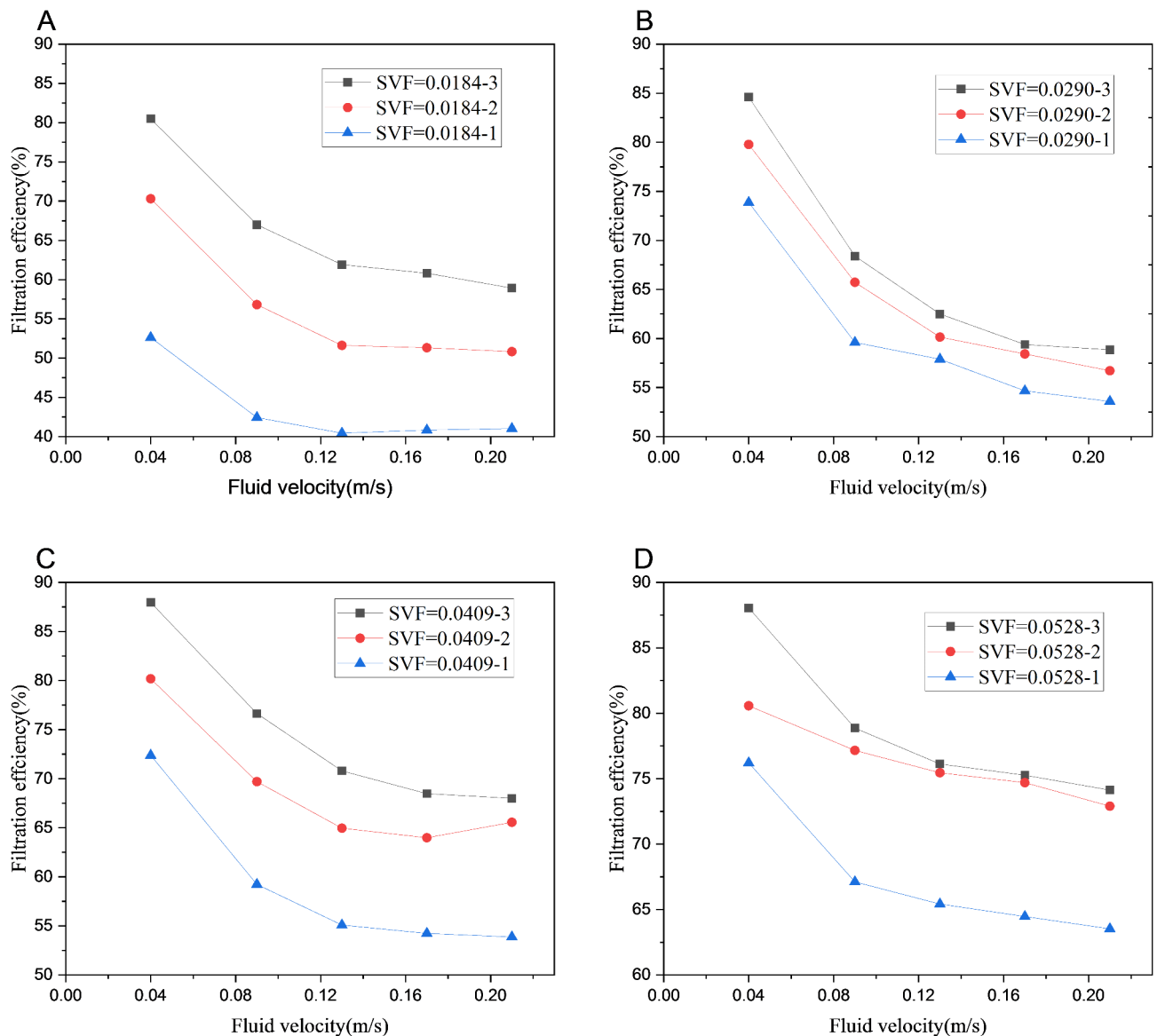


Fig. 5. Relationship between fiber pressure drop and SVF in different fluid velocity.

### The influence of SVF and layers on filtration efficiency

The filtration efficiency of all three layers of fiber media decreased with increasing fluid velocity at different SVF conditions. At the SVF of 0.0184, the filtration efficiency increased from 52.5% to 83.24% with layers of fibrous media increasing from 1 to 3 at the fluid velocity of 0.04 m/s; while the filtration efficiency decreased from 52.5% to 40% with the fluid velocity increasing from 0.04 m/s to 0.21 m/s at the same 1 layer of fibrous media in Fig. 6A. At the SVF of 0.0290, The filtration efficiency declined from 85% to 58.5% as the fluid velocity increased from 0.04 m/s to 0.21 m/s at the 3 layers of fibrous media; but the filtration efficiency increased from 73.5% to 85% with layers increasing from 1 to 3 in the fluid velocity of 0.04 m/s in Fig. 6B. At the SVF of 0.0409, the filtration efficiency increased from 72% to 87.5% with the layers increasing from 1 to 3 in the fluid velocity of 0.04 m/s; while the filtration efficiency decreased from 87.5% to 68% as the fluid velocity increased from 0.04 m/s to 0.21 m/s at the 3 layers of fibrous media in Fig. 6C. At the SVF of 0.0528, the filtration efficiency increased from 76% to 88% with the layers increasing from 1 to 3 in the fluid velocity of 0.04 m/s; while the filtration efficiency decreased from 88% to 74% as the fluid velocity increased from 0.04 m/s to 0.21 m/s at the 3 layers of fibrous media in Fig. 6D. Under the same layers of fibrous media, the filtration efficiency of the fibrous media increased with the higher SVF (from 0.0184 to 0.0528), agreed with field study<sup>52</sup>. At low fluid velocities, the captured particles adhered more stably to the surface of the fibrous media. As fluid velocity increased, particles were more likely to break away with the airflow rather than being collected, resulting in a drop in capture efficiency. SVF reflected the density of fibers within the fibrous media; for the same dust source, it was evident that dense fibers collected more dust than sparse fibers. This finding revealed how variations in SVF caused changes in the internal structure, making it simpler for particulate materials to be trapped by processes. However, as fluid velocity increased, efficiency declined. The increased fluid velocity damaged the structure of particulate matter,



**Fig. 6.** Filtration efficiency at different air velocities.

such as dendrites structure sticking to fibers, resulting in a loss in efficiency. According to the literature<sup>22,33</sup>, the effect of inertia collision was particularly obvious when the fluid velocity increased, leading the particles to travel in a straight line with the gas stream, raising the probability of particle-fiber collisions. However, the influence of deposited particles on fluid velocity was not been addressed. In this study, considering the particle deposition, the results were found that increasing fluid velocity would break the dendritic structure and allow the deposited particles to detach, leading to lowering filtration effectiveness.

### Influence of dust accumulation on pressure drop and filtration efficiency

#### Pressure drop

The effect of dust loading on filtering performance during the deposition process could be seen in Fig. 7, resulted in a high increase in efficiency and a small increase in pressure drop in the first stage (the dust loading from 20  $\text{mg}/\text{m}^3$  to 140  $\text{mg}/\text{m}^3$ ). As the dust loading rose, a stable cake structure formed within the filter media, and the efficiency progressively achieved dynamic stabilization. The pressure drop only increased from 5.74 Pa to 6.15 Pa with a growth rate of 15.83% in the first stage, whereas the growth became significantly faster in the second stage (the dust loading from 140  $\text{mg}/\text{m}^3$  to 1200  $\text{mg}/\text{m}^3$ ) the pressure drop increased from 6.15 Pa to 14.96 Pa with a growth rate of 143%, consistent with the results of Frising et al.<sup>53</sup>. The increase in dust loading during deposition could be substituted for the ESVF, which was introduced into Eq. (6) from Eqs. (11)–(12) to obtain Eq. (13) about the relationship between the pressure drop  $\Delta P$  and the dust loading ( $M_x$ ).

$$f(M_x) = \Delta P = K_0(K_1 + K_2 M_x)^{\frac{3}{2}} [1 + 56(K_1 + K_2 M_x)^3] \quad (13)$$

where  $K_0$ ,  $K_1$  and  $K_2$  were quantities independent of  $M_x$ .

The pressure curve was displayed as a function of dust loading using Eq. (13) (Fig. 7). In the initial stage of filtration,  $\Delta c$  was caused to rise for particles deposit and form dendrites structure across the filter media. As dust loading increased,  $\Delta c$  was led to gradually stabilize because particles accumulated on the filter media surface. These cakes were continuously compacted as the filtration process, as well as the filtration mechanism shifted from deep filtration to surface filtration and cake creation as the dust was loaded, resulting in a change in pressure, agreed with field study<sup>13</sup>.

#### Filtration efficiency

Figure 8 depicts the simulation of two fiber media (SVF=0.0528 and SVF=0.152) at a fluid velocity of 0.17 m/s. To validate the model's correctness, the deposition experiments were performed on a fiber medium with an SVF of 0.152 at an airflow of 3400  $\text{m}^3/\text{h}$  (fluid velocity=0.17 m/s). The efficiency of the filter changed as the dust

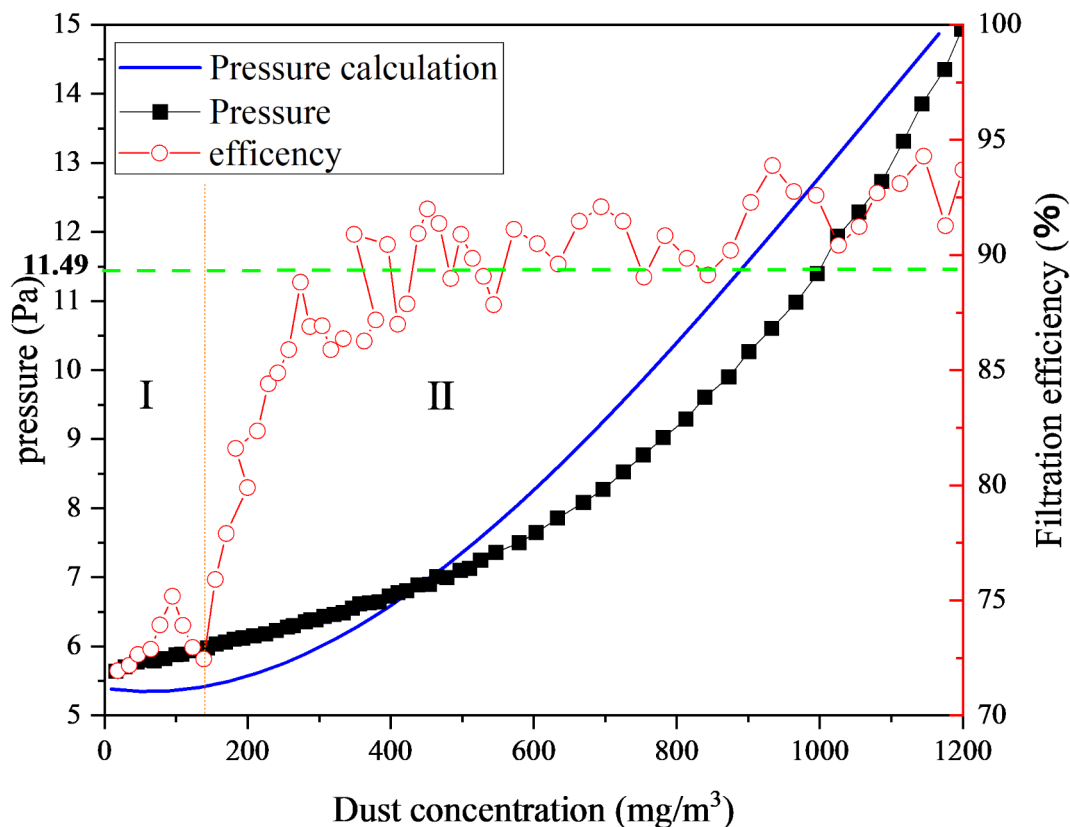


Fig. 7. Pressure drop and efficiency during dust loading.

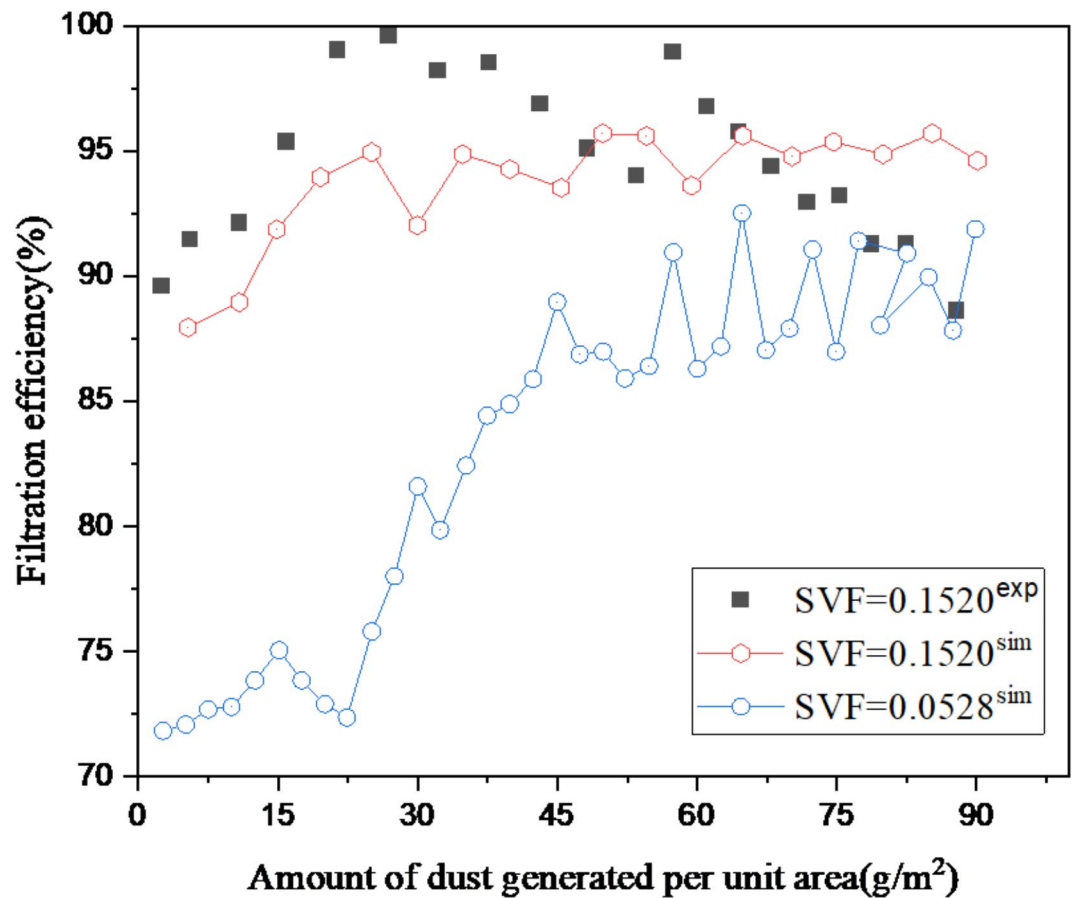


Fig. 8. Changes in the efficiency of the filtered media during dust loading.

loading increased (Fig. 8). Because the particles deposited on the surface of filter fibers could operate as a capture for the particles following the filter, the efficiency gradually increased with the filter accumulated dust, which was the phenomenon called “filter cake”<sup>36,54</sup>. Filter cake surfaces serve as a filtration function to collect the dust in the back and also serve as a new “fiber”, resulting in a smaller gap in the capture network, greater density, and increased SVF of the filter material.

According to the empirical formulas for filtration efficiency mentioned in Eqs. (10) and (11),  $g(\Delta c)$ , a function of the ESVF, was defined as Eq. (14).

$$g(\Delta c) = \eta = 1 - \exp\left(k_3 \frac{\Delta c}{1 - \Delta c}\right) \quad (14)$$

Where  $k_3$  is a constant (-15) in this condition. Efficiency increased and then stabilized when the comparable solid volume fraction rose. The concept of ESVF ( $\Delta c$ ) was introduced to explain the specific relationship between fiber filtration efficiency and SVF. The ESVF of the fibrous media would increase and stabilize at 0.16 with the dust-loading proceeding, and the efficiency of the fibrous media gradually stabilized without the same initial SVF (Fig. 9).

The number of particles deposited on fiber surfaces gradually increases with filtration time. During the early stage of filtration (Fig. 10  $T=1$ ms), the deposited particles are evenly distributed across the surface of the fibers. Then, with filtering, they gradually form a more distinct dendritic structure (Fig. 10  $T=5$ ms); at this moment, the particles have not entirely deposited on the fibers, but the majority have been caught by the dendrites. When the filtering period reaches a specific time (Fig. 10,  $T=15$ ms or  $T=20$ ms), more dendrites are created by decreasing the porosity, indicating that the agglomeration process is more visible, resulting in the formation of filter cake. However, the dendritic shape in the early stages of filtration improved filtration efficiency to some extent<sup>13</sup> (Fig. 10). But it was also relatively unstable since the dendritic structure was easily destroyed by mass particle inertia, and efficiency fluctuated with dendritic structure breakdown and reformation. As the large mass particles left<sup>52</sup>, the dendrite gradually became denser, and the efficiency rose until the filter was blocked and destroyed<sup>27</sup>.

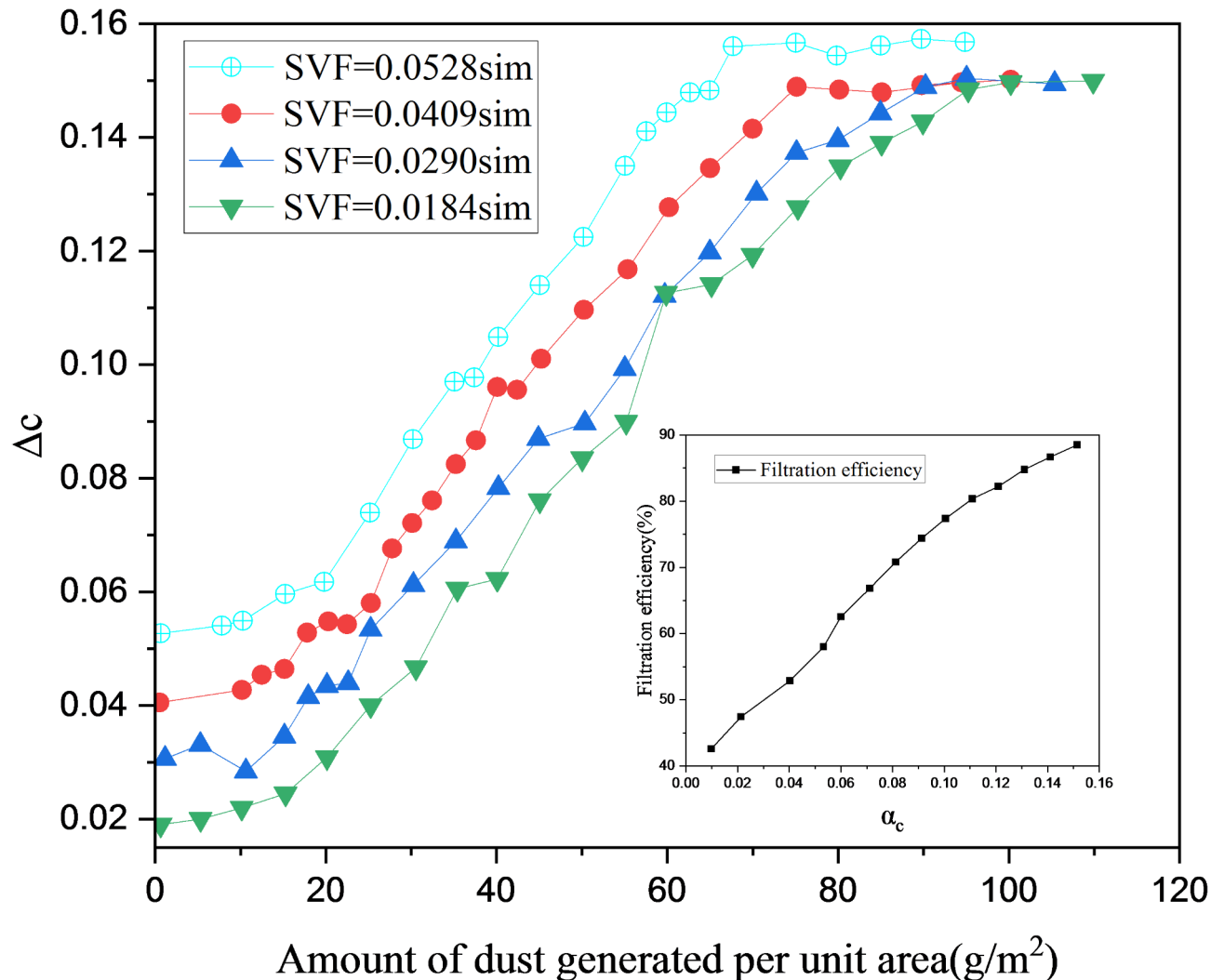


Fig. 9.  $\Delta c$  during dust loading

### The influence of particle size on filtration efficiency

Particle size affected filtration efficiency during the dust-holding process of the fiber media. According to ISO 12103-1, A2 experimental dust (mainly silica, doped with other mixtures,  $900 \text{ kg/m}^3$ )<sup>51,55</sup> was used in this experiment, and the particle size distribution was shown in Fig. 11.

Figure 11 showed the efficiency of the A2 dust particle compared to the empirical model at SVF = 0.0528. The filtration efficiency increased as particle size rose due to the inertial collision and interception effect (Fig. 11). This phenomenon had also been validated in the literature<sup>56</sup>. The efficiency in this paper was higher than in the Kuwabara empirical correlation. This phenomenon might be explained that the empirical formula for filtration efficiency was calculated based on single fibers, whereas the filtration media in this simulation was multifiber. Simultaneously, the total effect of many mechanisms resulted in the filter media's filtration efficiency on the particles. There might be a discrepancy between the simulated efficiency value and the empirical formula value because Eq. (9) only took into account inertia, diffusion, and interception. The study's particle size ranged from 1 to  $120 \mu\text{m}$ , and the particles' Brownian diffusion was extremely tiny. Despite this, the overall trend was consistent with the trend in the calculations of Eq. (9).

### Conclusions

This study examined the filter performance of dynamic processes of particle deposition by the CFD-DEM. A 3-D model of the fibrous media was established based on real F8 fibrous media. The effects of the SVF, filtration velocity, particle size and dust loading, and fiber diameter distribution on the filtration efficiency of fibrous media were studied. Pressure drop and filtration efficiency were positively correlated with SVF. Pressure drop increased with higher fluid velocity at one certain SVF. When the fluid velocity increased, the filtration efficiency reduced because the dendrites structure of particles on the fiber was destroyed. The filtration efficiency increased with the particle size of the particulate matter, because of the increased inertial impaction and interception of particles. The filtration efficiency increased from 73% to 92.5% with the increase in the dust generation

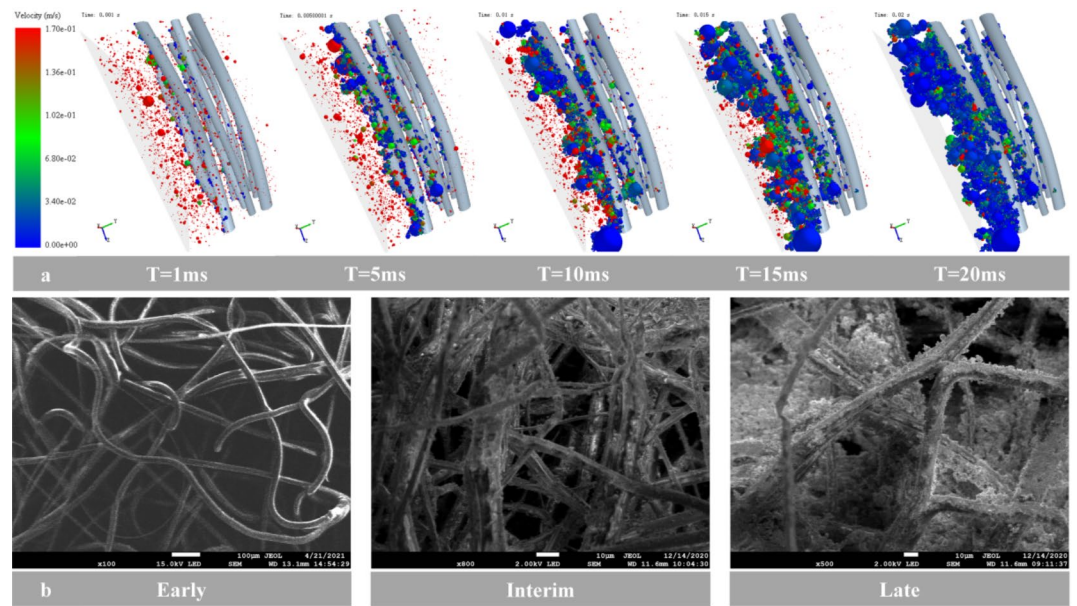


**Fig. 10.** Deposition of particles on fibrous media (Top: Simulation, Bottom: Experiment)(clean fiber media (Early), dust-loaded fiber media (11.49 Pa, twice the initial resistance) (Interim) and dust-loaded fiber media (15 Pa, the maximum pressure drop) (Late) by scanning electron microscopy (SEM) imaging.)

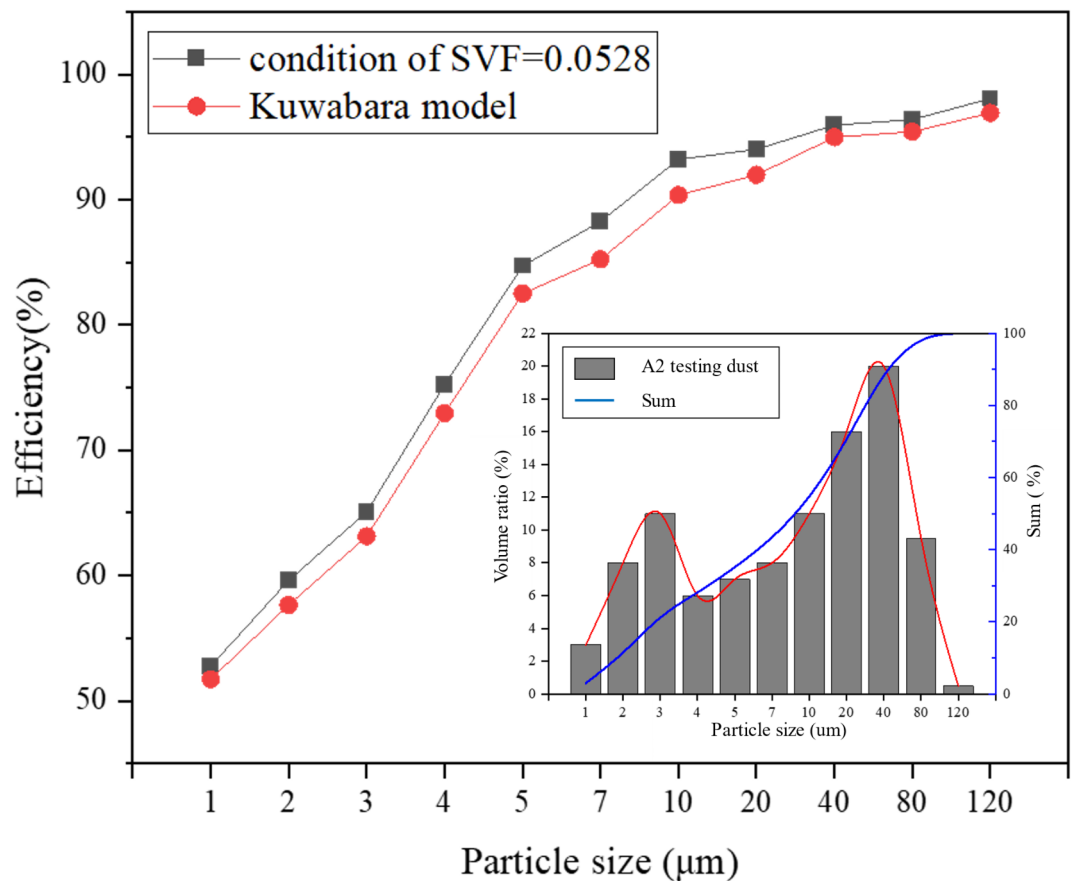


**Fig. 11.** Fractional efficiency of the fibrous media (SVF=0.0528).

concentration (from  $140\text{mg/m}^3$  to  $1000\text{ mg/m}^3$ ). The formula for the resistance and efficiency with the ESVF was provided as a function of dust holding capacity, along with the curves for the resistance and efficiency. The filtration efficiency first rose rapidly and then fluctuated resulting from changes in ESVF. Additionally, since the particulate matter in the real filtration process contained a range of components and behaviors, more research on multi-field coupling mixed with varied features should be required in the future.

## Data availability

Data is provided within the manuscript.

Received: 11 December 2024; Accepted: 10 March 2025

Published online: 01 September 2025

## References

- Sutherland, K. Choosing equipment: cleaning air and gas. *Filtr. Sep.* **44**, 16–19. [https://doi.org/10.1016/S0015-1882\(07\)70020-4](https://doi.org/10.1016/S0015-1882(07)70020-4) (2007).
- Thakur, R., Das, D. & Das, A. Electret air filters, *Sep. Purif. Rev.* **42**, 87–129. <https://doi.org/10.1080/15422119.2012.681094> (2013).
- Ji, L., Pei, J. & Liu, W. Long-term performance of fibrous ventilation/air-cleaner filters for particle removal. *Build. Environ.* **160**, 106222. <https://doi.org/10.1016/j.buildenv.2019.106222> (2019).
- Kuwabara, S. The forces experienced by randomly distributed parallel circular cylinders. *J. Phys. Soc. Japan.* **14**, 527–532 (1959).
- Keilany, Z. & Reviews, B. *Rev. Soc. Econ.* **36** 228–229. <https://doi.org/10.1080/00346767800000037>. (1978).
- Happel, J. Viscous flow relative to arrays of cylinders. *AIChE J.* **5**, 174–177. <https://doi.org/10.1002/aic.690050211> (1959).
- Zhang, X., Liu, J. & Liu, C. A novel slip-velocity model to simulate the filtration performance of nanofiber media. *Process. Saf. Environ. Prot.* **174**, 548–560. <https://doi.org/10.1016/j.psep.2023.04.034> (2023).
- Saleh A.M., Tafreshi, H. V. & Pourdeyhimi, B. An analytical approach to predict pressure drop and collection efficiency of dust-load pleated filters. *Sep. Purif. Technol.* **161**, 80–87. <https://doi.org/10.1016/j.seppur.2016.01.034> (2016).
- Bian, Y., Wang, S., Zhang, L. & Chen, C. Influence of fiber diameter, filter thickness, and packing density on PM2.5 removal efficiency of electrospun nanofiber air filters for indoor applications. *Build. Environ.* **170**, 106628. <https://doi.org/10.1016/j.buildenv.2019.106628> (2020).
- Pan, Z. et al. Study of structural factors of structure-resolved filter media on the particle loading performance with microscale simulation. *Sep. Purif. Technol.* **304**, 122317. <https://doi.org/10.1016/j.seppur.2022.122317> (2023).
- Li, S. et al. Influence of pleat geometry on the filtration and cleaning characteristics of filter media. *Sep. Purif. Technol.* **210**, 38–47. <https://doi.org/10.1016/j.seppur.2018.05.002> (2019).
- Zhou, Z. J. et al. Evaluation of characterization and filtration performance of air cleaner materials. *Int. J. Environ. Sci. Technol.* **18**, 2209–2220. <https://doi.org/10.1007/s13762-020-02966-9> (2021).
- Shu, Z., Qian, F. & Fang, C. Numerical simulation of particle Spatial distribution and filtration characteristic in the pleated filter media using openfoam. *Indoor Built Environ.* **0**, 1–14. <https://doi.org/10.1177/1420326X20931925> (2020).
- Zhang, X. & Liu, J. Operating resistance prediction of non-flat HEPA filters. *Powder Technol.* **408**, 117718. <https://doi.org/10.1016/j.powtec.2022.117718> (2022).
- Zhang, X., Liu, J., Liu, X. & Liu, C. Performance optimization of airliner cabin air filters. *Build. Environ.* **187**, 107392. <https://doi.org/10.1016/j.buildenv.2020.107392> (2021).
- Zhang, W., Deng, S., Wang, Y. & Lin, Z. Dust loading performance of the Ptfе HEPA media and its comparison with the glass fibre HEPA media. *Aerosol Air Qual. Res.* **18**, 1921–1931. <https://doi.org/10.4209/aaqr.2017.11.0481> (2018).
- Zhang, W., Deng, S., Wang, Y. & Lin, Z. Modeling the surface filtration pressure drop of PTFE HEPA filter media for low load applications. *Build. Environ.* **177**, 106905. <https://doi.org/10.1016/j.buildenv.2020.106905> (2020).
- Cao, B. et al. Pressure drop model for fibrous media in depth filtration: Coupling simulation of microstructure and CFD porous media during dust loading. *Build. Environ.* **202**, 108015. <https://doi.org/10.1016/j.buildenv.2021.108015> (2021).
- Wang, Q., Lin, X. & Chen, D. R. Effect of dust loading rate on the loading characteristics of high efficiency filter media. *Powder Technol.* **287**, 20–28. <https://doi.org/10.1016/j.powtec.2015.09.032> (2016).
- Yit, J. E., Yau, Y. H. & Chew, B. T. The influence of filtration velocity on the full-sized fibrous filter performance. *Indoor Built Environ.* **32**, 375–386. <https://doi.org/10.1177/1420326X221113446> (2023).
- Rao, N. & Faghri, M. Computer modeling of aerosol filtration by fibrous filters. *Aerosol Sci. Technol.* **8**, 133–156. <https://doi.org/10.1080/02786828808959178> (1988).
- Brown, R. C. Theory of airflow through filters modelled as arrays of parallel fibres. *Chem. Eng. Sci.* **48**, 3535–3543. [https://doi.org/10.1016/0009-2509\(93\)85009-E](https://doi.org/10.1016/0009-2509(93)85009-E) (1993).
- Wang, H., Zhao, H., Guo, Z., He, Y. & Zheng, C. Lattice Boltzmann method for simulations of gas-particle flows over a backward-facing step. *J. Comput. Phys.* **239**, 57–71. <https://doi.org/10.1016/j.jcp.2012.12.032> (2013).
- Tao, R., Yang, M. & Li, S. Effect of adhesion on clogging of microparticles in fiber filtration by DEM-CFD simulation. *Powder Technol.* **360**, 289–300. <https://doi.org/10.1016/j.powtec.2019.09.083> (2020).
- Chen, D. R., Pui, D. Y. H. & Liu, B. Y. H. Optimization of pleated filter designs using a finite-element numerical model. *Aerosol Sci. Technol.* **23**, 579–590. <https://doi.org/10.1080/02786829508965339> (1995).
- Kang, S., Lee, H., Kim, S. C., Chen, D. R. & Pui, D. Y. H. Modeling of fibrous filter media for ultrafine particle filtration. *Sep. Purif. Technol.* **209**, 461–469. <https://doi.org/10.1016/j.seppur.2018.07.068> (2019).
- Li, S. Q. & Marshall, J. S. Discrete element simulation of micro-particle deposition on a cylindrical fiber in an array. *J. Aerosol Sci.* **38**, 1031–1046. <https://doi.org/10.1016/j.jaerosci.2007.08.004> (2007).
- Xu, B., Wu, Y. & Cui, P. Semi-analytical and computational investigation of different dust loading structures affecting the performance of a fibrous air filter. *Particuology* **13**, 60–65. <https://doi.org/10.1016/j.partic.2013.05.004> (2014).
- Cao, B. et al. Investigation of the filtration performance for fibrous media: Coupling of a semi-analytical model with CFD on Voronoi-based microstructure. *Sep. Purif. Technol.* **251**, 117364. <https://doi.org/10.1016/j.seppur.2020.117364> (2020).
- Soltani, P., Johari, M. S. & Zarrebini, M. Effect of 3D fiber orientation on permeability of realistic fibrous porous networks. *Powder Technol.* **254**, 44–56. <https://doi.org/10.1016/j.powtec.2014.01.001> (2014).
- Fotovati, S., Hosseini, S. A., Vahedi Tafreshi, H. & Pourdeyhimi, B. Modeling instantaneous pressure drop of pleated thin filter media during dust loading. *Chem. Eng. Sci.* **66**, 4036–4046. <https://doi.org/10.1016/j.ces.2011.05.038> (2011).
- Théron, F., Joubert, A. & Le Coq, L. Numerical and experimental investigations of the influence of the pleat geometry on the pressure drop and velocity field of a pleated fibrous filter. *Sep. Purif. Technol.* **182**, 69–77. <https://doi.org/10.1016/j.seppur.2017.02.034> (2017).
- Saleh, A. M., Fotovati, S., Vahedi Tafreshi, H. & Pourdeyhimi, B. Modeling service life of pleated filters exposed to poly-dispersed aerosols. *Powder Technol.* **266**, 79–89. <https://doi.org/10.1016/j.powtec.2014.06.011> (2014).

34. Schilling, M., Schütz, S. & Piesche, M. Numerical simulation of the transport and deposition behaviour of particles on filter fibres using Euler-Lagrange method and coupling of CFD and DEM. *AIP Conf. Proc.* **1207**, 789–795. <https://doi.org/10.1063/1.3366464> (2010).
35. Sheng, Y., Ren, Q., Zhang, L. & Wang, Y. Modeling and simulation of DEHS aerosol filtration by a three-dimensional knitted spacer air filter. *Build. Environ.* **186**, 107365. <https://doi.org/10.1016/j.buildenv.2020.107365> (2020).
36. Qian, F., Huang, N., Lu, J. & Han, Y. CFD-DEM simulation of the filtration performance for fibrous media based on the mimic structure. *Comput. Chem. Eng.* **71**, 478–488. <https://doi.org/10.1016/j.compchemeng.2014.09.018> (2014).
37. Sheng, Y., Wang, M., Zhang, L. & Ren, Q. Analysis of filtration process of 3-D mesh spacer filter by using CFD-DEM simulation. *Powder Technol.* **396**, 785–793. <https://doi.org/10.1016/j.powtec.2021.11.034> (2022).
38. Vivacqua, V., López, A., Hammond, R. & Ghadiri, M. DEM analysis of the effect of particle shape, cohesion and strain rate on powder rheometry. *Powder Technol.* **342**, 653–663. <https://doi.org/10.1016/j.powtec.2018.10.034> (2019).
39. Dong, M., Li, J., Shang, Y. & Li, S. Numerical investigation on deposition process of submicron particles in collision with a single cylindrical fiber. *J. Aerosol Sci.* **129**, 1–15. <https://doi.org/10.1016/j.jaerosci.2018.12.001> (2019).
40. Cheng, K. et al. CFD-DEM simulation of particle deposition characteristics of pleated air filter media based on porous media model. *Particuology* **72**, 37–48. <https://doi.org/10.1016/j.partic.2022.02.003> (2023).
41. Di Renzo, A., Cello, F., Di, F. P. & Maio, S. Simulation of the layer inversion phenomenon in binary liquid-fluidized beds by DEM-CFD with a drag law for polydisperse systems. *Chem. Eng. Sci.* **66**, 2945–2958. <https://doi.org/10.1016/j.ces.2011.03.035> (2011).
42. Johnson, K. L., Kendall, K. & Roberts, A. D. Surface energy and the contact of elastic solids. *Proc. R Soc. Lond. Math. Phys. Sci.* **324**, 301–313. <https://doi.org/10.1098/rspa.1971.0141> (1971).
43. Chu, K. W., Wang, B., Yu, A. B. & Vince, A. CFD-DEM modelling of multiphase flow in dense medium cyclones. *Powder Technol.* **193**, 235–247. <https://doi.org/10.1016/j.powtec.2009.03.015> (2009).
44. Pourdeyhimi, B., Mazé, B. & Tafreshi, H. V. Simulation and analysis of unbonded nonwoven fibrous structures. *J. Eng. Fiber Fabr.* **1**, 155892500600100. <https://doi.org/10.1177/155892500600100204> (2006).
45. Zhang, X., Liu, J. & Wu, H. Adjustable fiber structure design for precise aerosol filtration. *Powder Technol.* **428**, 118881. <https://doi.org/10.1016/j.powtec.2023.118881> (2023).
46. Wang, Q., Maze, B., Tafreshi, H. V. & Pourdeyhimi, B. A case study of simulating submicron aerosol filtration via lightweight spun-bonded filter media. *Chem. Eng. Sci.* **61**, 4871–4883. <https://doi.org/10.1016/j.ces.2006.03.039> (2006).
47. Zhu, X., Qian, F., Lu, J. & Zhang, H. Numerical study of the solid volume fraction and pressure drop of fibrous media by response surface methodology. *Chem. Eng. Technol.* **36**, 788–794. <https://doi.org/10.1002/ceat.201200512> (2013).
48. Zhu, S. W., Kato, S. & Yang, J. H. Study on transport characteristics of saliva droplets produced by coughing in a calm indoor environment. *Build. Environ.* **41**, 1691–1702. <https://doi.org/10.1016/j.buildenv.2005.06.024> (2006).
49. Davies, C. N. The separation of airborne dust and particles. *Proc. Inst. Mech. Eng. Part. B Manag. Eng. Manuf.* **1**, 185–213. <https://doi.org/10.1177/095440545300100113> (1953).
50. Zhang, X. & Liu, J. Simplified model for the calculation of the particle capture process in air filter media. *Chem. Eng. Sci.* **249**, 117358. <https://doi.org/10.1016/j.ces.2021.117358> (2022).
51. EN779:2012 Particulate air filters for general ventilation-Determination of the filtration performances[S]. 16–22. (2012).
52. Yue, C., Zhang, Q. & Zhai, Z. Numerical simulation of the filtration process in fibrous filters using CFD-DEM method. *J. Aerosol Sci.* **101**, 174–187. <https://doi.org/10.1016/j.jaerosci.2016.08.004> (2016).
53. Frising, T., Thomas, D., Bémer, D. & Contal, P. Clogging of fibrous filters by liquid aerosol particles: Experimental and phenomenological modelling study. *Chem. Eng. Sci.* **60**, 2751–2762. <https://doi.org/10.1016/j.ces.2004.12.026> (2005).
54. Qian, F., Huang, N., Zhu, X. & Lu, J. Numerical study of the gas-solid flow characteristic of fibrous media based on SEM using CFD-DEM. *Powder Technol.* **249**, 63–70. <https://doi.org/10.1016/j.powtec.2013.07.030> (2013).
55. Ko, G. H. & Ryou, H. S. Modeling of droplet collision-induced breakup process. *Int. J. Multiph. Flow* **31**, 723–738. <https://doi.org/10.1016/j.ijmultiphaseflow.2005.02.004> (2005).
56. Callé, S., Contal, P., Thomas, D., Bémer, D. & Leclerc, D. Description of the clogging and cleaning cycles of filter media. *Powder Technol.* **123**, 40–52. [https://doi.org/10.1016/S0032-5910\(01\)00430-2](https://doi.org/10.1016/S0032-5910(01)00430-2) (2002).

## Author contributions

Y.L. and J.C. and P.C. wrote the main manuscript text as well as the validation treatment study data; Y.L. and J.C. and W.Y. reviewed the main manuscript.

## Funding

This research was funded by the Tianjin Science and Technology Program Project (No. 19YFZCSN01120); the Tianjin Science and Technology Program Project (No. 18YFZCSF00630), and the Graduate Student Research Innovation Program of Tianjin (No. 2022SKYZ220).

## Declarations

## Competing interests

The authors declare no competing interests.

## Additional information

**Correspondence** and requests for materials should be addressed to Y.L.

**Reprints and permissions information** is available at [www.nature.com/reprints](http://www.nature.com/reprints).

**Publisher's note** Springer Nature remains neutral with regard to jurisdictional claims in published maps and institutional affiliations.

**Open Access** This article is licensed under a Creative Commons Attribution-NonCommercial-NoDerivatives 4.0 International License, which permits any non-commercial use, sharing, distribution and reproduction in any medium or format, as long as you give appropriate credit to the original author(s) and the source, provide a link to the Creative Commons licence, and indicate if you modified the licensed material. You do not have permission under this licence to share adapted material derived from this article or parts of it. The images or other third party material in this article are included in the article's Creative Commons licence, unless indicated otherwise in a credit line to the material. If material is not included in the article's Creative Commons licence and your intended use is not permitted by statutory regulation or exceeds the permitted use, you will need to obtain permission directly from the copyright holder. To view a copy of this licence, visit <http://creativecommons.org/licenses/by-nc-nd/4.0/>.

© The Author(s) 2025